PLOS ONE
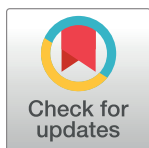
Incorporating radiomic feature of pretreatment ^{18}F-FDG PET improves survival stratification in patients with EGFR-mutated lung adenocarcinoma

Yu-Hung Chen [1,2], Tso-Fu Wang[2,3], Sung-Chao Chu[2,3], Chih-Bin Lin[4], Ling-Yi Wang[5], Kun-Han Lue[6], Shu-Hsin Liu[1,6], Sheng-Chieh Chan[1,2]*

1 Department of Nuclear Medicine, Hualien Tzu Chi Hospital, Buddhist Tzu Chi Medical Foundation, Hualien, Taiwan, 2 Department of Medicine, College of Medicine, Tzu Chi University, Hualien, Taiwan, 3 Department of Hematology and Oncology, Hualien Tzu Chi Hospital, Buddhist Tzu Chi Medical Foundation, Hualien, Taiwan, 4 Department of Internal Medicine, Hualien Tzu Chi Hospital, Buddhist Tzu Chi Medical Foundation, Hualien, Taiwan, 5 Epidemiology and Biostatistics Consulting Center, Department of Medical Research and Department of Pharmacy, Tzu Chi General Hospital, Hualien, Taiwan, 6 Department of Medical Imaging and Radiological Sciences, Tzu Chi University of Science and Technology, Hualien, Taiwan

* williamsm.tw@gmail.com

Abstract

Background

To investigate the survival prognostic value of the radiomic features of ^{18}F-FDG PET in patients who had EGFR (epidermal growth factor receptor) mutated lung adenocarcinoma and received targeted TKI (tyrosine kinase inhibitor) treatment.

Methods

Fifty-one patients with stage III-IV lung adenocarcinoma and actionable EGFR mutation who received first-line TKI were retrospectively analyzed. All patients underwent pretreatment ^{18}F-FDG PET/CT, and we calculated the PET-derived radiomic features. Cox proportional hazard model was used to examine the association between the radiomic features and the survival outcomes, including progression-free survival (PFS) and overall survival (OS). A score model was established according to the independent prognostic predictors and we compared this model to the TNM staging system using Harrell's concordance index (c-index).

Results

Forty-eight patients (94.1%) experienced disease progression and 41 patients (80.4%) died. Primary tumor SUV entropy > 5.36, and presence of pleural effusion were independently associated with worse OS (both $p < 0.001$) and PFS ($p = 0.001$, and 0.003, respectively). We used these two survival predictors to devise a scoring system (score 0–2). Patients with a score of 1 or 2 had a worse survival than those with a score of 0 (HR for OS: 3.6, $p = 0.006$ for score 1, and HR: 21.8, $p < 0.001$ for score 2; HR for PFS: 2.2, $p = 0.027$ for

score 1 and HR: 8.8, *p* < 0.001 for score 2). Our scoring system surpassed the TNM staging system (c-index = 0.691 versus 0.574, *p* = 0.013 for OS, and c-index = 0.649 versus 0.517, *p* = 0.004 for PFS).

Conclusions

In this preliminary study, combining PET radiomics with clinical risk factors may improve survival stratification in stage III-IV lung adenocarcinoma with actionable EFGR mutation. Our proposed scoring system may assist with optimization of individualized treatment strategies in these patients.

Introduction

The incidence of lung cancer is the highest among all types of cancers. Lung cancer is also the leading cause of cancer-related deaths worldwide [1]. In the United States, approximately 230000 new lung cancer cases, and nearly 143000 lung cancer related deaths were reported in the 2019 cancer statistics [1, 2]. Adenocarcinoma is currently the most common histopathological subtype of lung cancer, and the incidence is rising [3]. The majority of lung adenocarcinoma cases present as metastatic disease upon diagnosis, and the prognosis among these patients is grim [1–4]. Fortunately, several targetable driver mutations have been discovered, and the use of the corresponding targeted therapeutic agents has significantly improved the prognosis of metastatic lung adenocarcinoma [5–8]. Among these targetable driver mutations, epidermal growth factor receptor (EGFR) mutation is the most common, and many effective tyrosine kinase inhibitors (TKIs) have been introduced [5, 6]. Although novel TKIs for EGFR mutation have emerged, 20%–40% of patients are non-responsive to TKI. Even though approximately 58%–83% of the cases are responsive initially, 50%–65% of cases will acquire resistance within 1 year [6]. Currently, drug resistance in patients with EGFR mutation cannot be accurately anticipated; as such, a reliable prediction tool is an imperative and unmet need [9].

^{18}F-fluorodeoxyglucose (^{18}F-FDG) positron emission tomography (PET) is an imaging modality that is capable of spotting altered glycolytic activity. It has been used widely as a staging, re-staging, and response evaluation tool for lung adenocarcinoma [10, 11]. Literature has shown that several ^{18}F-FDG PET derived semiquantitative parameters such as the standardized uptake value (SUV), metabolic tumor volume (MTV), and total lesion glycolysis (TLG), are associated with the prognosis in patients with non-small cell lung cancer [12–14]. In addition, texture analysis provides a new way of featuring for ^{18}F-FDG PET, and some reports have shown an association between the texture features of ^{18}F-FDG PET and the tumor control and survival of patients with lung cancer [15–17]. The texture features of ^{18}F-FDG PET allow us to assess the heterogeneity of a tumor, which is driven by genomic diversity that allows the tumors to adapt and fight against treatments. Therefore, tumor heterogeneity is associated with the prognosis of cancers [18–21]. Texture features and semiquantitative parameters are radiomic features of ^{18}F-FDG PET. Distinct from the current cancer staging system and clinical risk factors, which focus more on the description of the disease extent or invasiveness, radiomics portrays more about the tumor biology and heterogeneity [4, 22, 23]. In this context, radiomics may complement the prognostic strength of the current clinical risk factors.

We conducted this study to investigate the utility of radiomic features of ^{18}F-FDG PET in predicting the survival in patients with primary advanced EGFR-mutated lung adenocarcinoma treated with TKIs.

Materials and methods

Study population

The Research Ethics Committee of Hualien Tzu Chi Hospital, Buddhist Tzu Chi Medical Foundation approved the protocol of this retrospective study (IRB109-010-B). The requirement of informed consent for this study was waived. We retrospectively enrolled patients with newly diagnosed EGFR mutated lung adenocarcinoma from January 2010 to December 2014. All participants had pathologically proven lung adenocarcinoma and had undergone serial examinations for staging at the initial diagnosis; these included contrast-enhanced CT of the chest to upper abdomen, ^{18}F-FDG PET/CT, and/or gadolinium-enhanced MRI of the brain. The staging was designated according to the 7th edition of the American Joint Committee on Cancer (AJCC) staging manual [4]. Patients with an AJCC stage of III or IV and an active EGFR mutation in exon 18, 19, 20, or 21 were included. All patients received EGFR targeting TKIs (Gefitinib, Erlotinib, or Afatinib) as the first-line treatment. Finally, 51 patients were included and followed until August 2019. The mutational analysis of EGFR was performed from the formalin-fixed, paraffin-embedded tissues of histopathologically confirmed lung adenocarcinoma. Mutations in EGFR were analyzed using an EGFR RGO Kit (Qiagen, Hilden, Germany). The choice of TKI was based on the decision of the attending physician. The examination findings were discussed at a multidisciplinary cancer conference convened by our thoracic oncology research group.

Imaging protocol for ^{18}F-FDG PET

All participants in our study fasted for at least 4 hours before ^{18}F-FDG injection (400 MBq). The ^{18}F-FDG PET/CT scans were acquired with the use of a GE Discovery ST PET/CT unit (Discovery ST16; GE Healthcare, Milwaukee, WI, USA). The PET/CT system was equipped with a PET unit having 10080 bismuth germanate crystals in 24 rings and a 16-detector row transmission CT unit (912 detectors/row). First, we acquired a transmission CT scan. The voltage and the current of the tube were 120 kV and 120 mA, respectively. The pitch of the transmission CT was 1.75. Image sampling was conducted using the helical mode with a helical thickness of 3.75 mm. The image reconstruction matrices were 512 × 512. No iodinated contrast material was administered for all transmission CT images. We obtained the PET images between 40 and 60 min after intravenous administration of radiotracer from the vertex to mid-thigh. The scanning time was 3.0 min for each table position (15 cm per table position with a 3-cm overlap for every contiguous frame). We used the transmission CT to perform attenuation correction for the PET images. The image reconstruction filter was ordered-subset expectation maximization iterative reconstruction algorithm (2 iterations and 21 subsets; matrix size, 128 × 128).

The analysis of PET images

We used the PMOD 4.0 software package (PMOD Technologies Ltd., Zurich, Switzerland) to display the ^{18}F-FDG PET/CT images and to perform the semiquantitative analysis. For semiquantitative analysis, we first identified the primary tumor of lung cancer on the ^{18}F-FDG PET/CT image. An experienced nuclear medicine physician then drew a volume-of-interest for the primary tumor. The SUV of ^{18}F-FDG PET was calculated and normalized based on the body weight:

$$SUV = \frac{(\text{decay} - \text{corrected activity [kBq] per milliliter of tissue volume})}{(\text{injected FDG activity [kBq]/body weight in g})}$$

We used an SUV threshold value of 2.5 for contouring the primary tumor inside the boundary

of the volume-of-interest [17, 24]. The PMOD 4.0 software automatically generated the contour margin around the primary tumor inside the boundary. The voxels indicating the SUV value of > 2.5 within the contour margin were used to define the MTV. The mean SUV within the contour margin was automatically generated. The TLG was then calculated based on the following formula:

$$TLG = \text{mean SUV} \times \text{MTV}$$

We used the contour margin of the primary tumor MTV to perform radiomic analysis. We selected three matrices to extract radiomic features from ^{18}F-FDG PET images in our study, included SUV histogram analysis, the gray-level co-occurrence matrix (GLCM), and the gray-level size-zone matrix (GLSZM) [25–27]. For the analysis of GLCM and GLSZM, the ^{18}F-FDG radioactivity uptake within the contour margin was resampled into 64 different values (bin number of 64) [17, 26, 28]. Subsequently, the radiomic features were computed as described in the previous studies [25–27]. Desseroit et al. reported the test-retest variabilities for the image features calculated from the SUV histogram, the GLCM, and the GLSZM in patients with non-small cell lung cancer. They found that the SUV entropy, the sum entropy, and small area emphasis (SAE) showed the least test-retest variability among the SUV histogram, the GLCM, and the GLSZM, respectively [29]. Therefore, we choose to use these three radiomic features for analysis in our study. The SUV entropy was defined as the uncertainty measure of the intensity distribution within the contour margin. P(i) indicated the probability of distinct resampled values and Ng represented the total number of discrete intensity levels within the contour margin. The ε is an arbitrarily small positive number ($\approx 2.2 \times 10^{-16}$). The calculation of SUV entropy was as follows:

$$SUV\ entropy = -\sum_{i=1}^{Ng} P(i)\log2(P(i) + \varepsilon)$$

From GLCM, we extracted sum entropy (gray-level co-occurrence matrix sum entropy). When GLCM(i, j) represents the probability that a voxel intensity i is neighbor to another voxel of intensity j, and represents to be the discrete intensity levels within the contour margin. Px+y(k) can be determined as follows:

$$Px + y(k) = \sum_{i=1}^{Ng}\sum_{j=1}^{Ng} GLCM(i,j)$$

The k was $i + j$, and k = 2, 3, . . ., 2Ng. The sum entropy was calculated as follows:

$$Sum\ entropy = -\sum_{k=2}^{2Ng} Px + y(k)\log2(Px + y(k) + \varepsilon)$$

Among the GLSZM parameters, SAE was selected for analysis. The matrix indicated how frequently a voxel of resampled intensity i was a size of j voxels. Nz represents the number of zones in the contour margin, GLSZM(i,j) represents the probability of the intensity i being a zone size of j, while Ng and Ns represent the discrete intensity levels and the number of discrete zone sizes in the contour margin, respectively. The SAE was calculated as follows:

$$SAE = \frac{1}{Nz}\sum_{i=1}^{Ng}\sum_{j=1}^{Ns} \frac{GLSZM(i,j)}{j2}$$

We summarized the procedures of the radiomic analysis in Fig 1. The software used to execute the aforementioned radiomic features was Pyradiomics 2.2.0 [30].
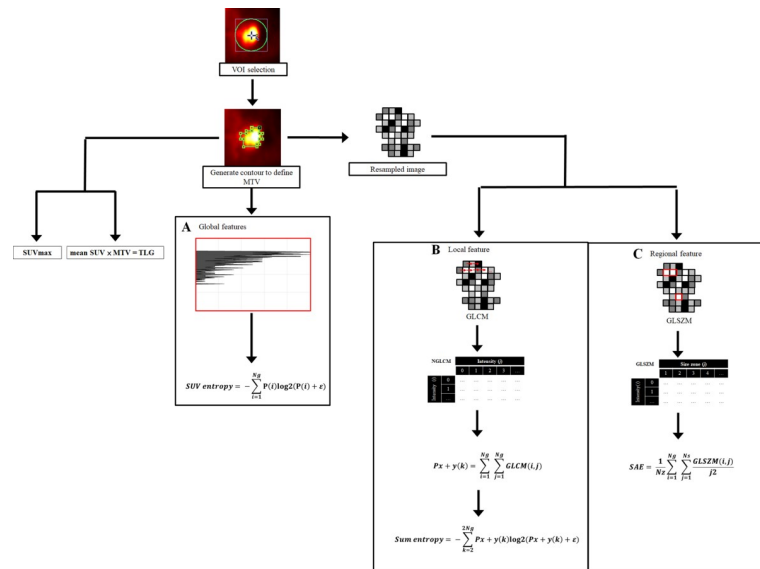
Fig 1. The method of radiomic analysis of ^{18}F-FDG PET images.

We first placed a VOI to include the primary tumor, and then an SUV threshold value of 2.5 was used for contouring. SUV histogram and two matrices were used in our study: one for local feature, and one for regional feature. VOI: Volume-of-interest, SUV: Standardized uptake value, MTV: Metabolic tumor volume, GLCM: Gray-level co-occurrence matrix, GLSZM: Gray-level size zone matrix, Pi: Probability of distinct resampled values, Ng: The total number of discrete intensity levels within contour margin, ε: An arbitrarily small positive number ($\approx 2.2 \times 10^{-16}$), GLCM($i,j$): The probability that a voxel of intensity i is neighbor to another voxel of intensity j; $k = i + j$, and $k = 2, 3, \ldots, 2$Ng, SAE: Small area emphasis, Nz: Number of zones in the contour margin, Ns: Number of discrete zone sizes in the contour margin, GLSZM(i,j): The probability of the intensity i being a zone size of j.

Follow-up of study patients

The results of the imaging study and the treatment strategies were discussed at a conference held by the thoracic oncology research group at our center. For lesions that were indicative of malignancy, image-guided biopsies were performed whenever possible. The patients were kept under close clinical and imaging follow-up if biopsy of a suspicious lesion was not feasible or if it yielded a negative result in a patient with equivocal or positive imaging findings. We followed-up the patient at the outpatient clinic at one-month interval, and we regularly performed thoracic-to-abdominal contrast-enhanced CT at 3-month intervals. When signs of symptoms of disease progression emerged, Contrast-enhanced CT, MRI of the brain and biopsy were performed. The treatment response to TKIs was classified as complete response, partial response, stable disease or progressive disease according to RECIST 1.1 criteria based on serial image studies [31]. New bloody effusion or a change from negative to positive fluid cytology was determined as disease progression.

Data analysis

Analysis of survival outcome. All patients were followed-up until death or August 2019 (whichever occurred first). We expressed the demographic data as a frequency or mean and

standard deviation, as appropriate. The overall survival (OS) was calculated from the date of diagnosis to the date of death or censored at the date of the last follow-up for surviving patients. Progression-free survival (PFS) was defined as the time between the start of TKI treatment and the date of disease progression (e.g., growth of a residual tumor or development of new metastatic lesion) or the date of death or censoring at the date of the last follow-up. The cut-off values for continuous variables were determined using the log-rank test based on the OS rates observed in the entire study cohort. We selected the cut-off values with the greatest chi-square value to be the optimal cut-off for each continuous variable [32]. An example of the operationalization of the cut-off value is shown in the S1 Fig. The optimal cut-off values for SUVmax, TLG, SUV entropy, sum entropy, and SAE were 6.75, 101, 5.36, 5.8, and 0.845, respectively. The association of the study variables with the survival outcomes was tested using the univariate and multivariate Cox regression analysis. We first examined the effect of each individual variable on the survival outcomes with the univariate analysis. Subsequently, the multivariate Cox regression analysis was used to identify the independent survival predictors. We expressed the results of the survival analysis as hazard ratios (HR) and 95% confidence intervals.

Model development. We established a scoring system to predict the OS and PFS based on the results of the multivariate Cox regression model. The presence of each independent survival predictor was designated a score of 1, and the absence of survival risk factor was assigned a score 0. For example, a patient with a score of 1 had one independent risk factor. We examined and compared the performance of our scoring system and the traditional AJCC staging system using the Kaplan-Meier curve method, log-rank test, and Harrell's concordance index (c-index) [33].

Model validation. The survival prediction model was validated using a bootstrapping validation method. The validation process was performed with 1000 bootstrap samples. The results of bootstrapping validation were expressed as bias with 95% confidence interval, standard error, and significance (*p*-value). Statistical analysis was performed using R-3.4.2 for Windows. The "compareC" package was applied to compare two correlated c-indices with a right-censored survival outcome. A two-tailed *p*-value of < 0.05 was considered statistically significant.

Results

Patient demographics

We summarized the distribution of patient characteristics of our study in the Table 1. A total of 39 (76.5%) patients were initially diagnosed with stage IV disease, 9 (17.6%) with stage IIIB disease, and 3 (5.9%) with stage IIIA disease. The three patients with stage IIIA status did not receive surgery as the primary treatment because of a poor pulmonary function test and/or advanced age. Twenty-six (51.0%) patients had L858R, 23 (45.0%) had a deletion in exon 19, and the other 2 patients had uncommon mutations; one with a S768I mutation and the other had a complex G719X mutation including G719A, G719S, G719C, and L861Q. The overall median follow-up period was 27.7 months (range 3.2–99.1 months) for all patients and 63.8 months (range 2.7.7–99.1 months) for the remaining 10 surviving patients. Forty-eight patients (94.1%) experienced disease progression during TKI treatment. A total of 41 (80.4%) patients had died by the time of the last follow-up. The 3-year OS rate and the 3-year PFS rate were 38.5% and 10.7%, respectively. The mean ± SD of the SUVmax and TLG values were 9.3 ± 3.65 and 216.5 ± 254.86, respectively. In terms of the radiomic features, the mean ± SD of the SUV entropy, sum entropy, and SAE were 5.3 ± 0.41, 5.8 ± 0.86 and 0.82 ± 0.590, respectively. A total of 44 (86.3%) patients experienced at least a partial response. The treatment response of first line TKI in 3 patients was stable disease, while the disease was progressive in 4 patients (Table 1).

Table 1. Baseline patient characteristics (n = 51).

Variable	Value
Age, years, mean ± SD	69 ± 9.0
Sex, n (%)	
Male	29 (59.6)
Female	22 (43.1)
Cigarette smoking, n (%)	
Ever smoker	21 (41.2)
Never smoker	30 (58.8)
Mutation type of EGFR	
Deletion 19	23 (45.0)
L858R	26 (51.0)
G719X	1 (2.0)
S768I	1 (2.0)
T classification, n (%)[a]	
T1	4 (7.8)
T2	16 (31.4)
T3	10 (19.6)
T4	21 (41.2)
N classification, n (%)[a]	
N0	7 (13.7)
N1	2 (4.0)
N2	17 (33.3)
N3	25 (49.0)
M classification, n (%)[a]	
M0	12 (23.5)
M1a	19 (37.3)
M1b	20 (39.2)
Overall stage, n (%)[a]	
Stage IIIA	3 (5.9)
Stage IIIB	9 (17.6)
Stage IV	39 (76.5)
Pleural effusion, n (%)	20 (39.2)
Lung to lung metastasis, n (%)	19 (37.3)
Hepatic metastasis, n (%)	6 (11.8)
Skeletal metastasis, n (%)	14 (27.5)
Brain metastasis, n (%)	6 (11.8)
First line TKI, n (%)	
Gefitinib	35 (68.6)
Erlotinib	12 (23.5)
Afatinib	4 (7.8)
Time from ^{18}F-FDG PET to TKI treatment, day, median (IQR)	8 (24)
Response of treatment, n (%)[b]	
Complete remission	1 (2.0)
Partial response	43 (84.3)
Stable disease	3 (5.9)
Progressive disease	4 (7.8)

SD: Standard deviation, EGFR: Epidermal growth factor receptor, TKI: tyrosine kinase inhibitor, IQR: interquartile range.

[a]Staging was based on the 7th American Joint Committee on Cancer system.

[b]Response assessment was based on RECIST 1.1 criteria.

https://doi.org/10.1371/journal.pone.0244502.t001

Univariate and multivariate Cox regression analysis

The median OS was 27.7 months (range, 3.2–99.1 months), and the median PFS was 14.1 months (range, 0–98.8 months). We summarized the results of the univariate and multivariate Cox regression analyses for the various study variables in the Table 2. The univariate analysis showed that poor OS was significantly associated with M1 status, presence of pleural effusion, presence of hepatic metastasis, a primary tumor SUVmax > 6.75, TLG > 101, a SUV entropy > 5.36, a sum entropy > 5.8, and a SAE ≤ 0.845. On the other hand, presence of pleural effusion and a SUV entropy > 5.36 were significantly associated with shorter PFS. The significant clinical and imaging variables in the univariate analysis were fitted into the multivariate Cox regression model. After multivariate analysis, the presence of pleural effusion, and a primary tumor SUV entropy > 5.36 were independent risk factors for both shorter OS and shorter PFS.

We devised a scoring system for predicting OS and PFS based on the number of independent risk factors present (presence of pleural effusion and primary tumor SUV entropy > 5.36). The presence or absence of each independent prognosticator was designated a score of 1 or 0, respectively, resulting in scores ranging from 0 to 2. Fig 2 demonstrates the value of this scoring system for stratifying OS and PFS in patients with EGFR-mutated lung adenocarcinoma. Compared with patients with a score of 0, the OS rates were worse in patients with a score of 1 (HR: 3.6, $p = 0.006$) and much worse in those with a score of 2 (HR: 21.8, $p < 0.001$). In the survival analysis of PFS, the PFS rates were also worse in patients with a score of 1 (HR: 2.2, $p = 0.027$) and much worse in those with a score of 2 (HR: 8.8, $p < 0.001$). Our survival prediction model outperformed the conventional TNM staging system and the survival stratification according to EGFR mutation status (Fig 3 and Table 3). Our model showed higher, yet non-statistically significant c-indices than the RECIST response assessment.

Bootstrapping validation

We used the bootstrap method to validate our survival prediction model. The S1 Table presents the results of the bootstrap validation. The β estimates of the two variables (presence of pleural effusion and primary tumor SUV entropy > 5.36) were still statistically significant in predicting both OS and PFS in the bootstrap results.

Discussion

Approximately 50%–65% of patients with EGFR-mutated lung adenocarcinoma will acquire resistance within 1 year despite initial response to TKI therapy, and eventually die of this disease [6]; thus, a more accurate prediction tool is currently an imperative need. ^{18}F-FDG PET has shown some value in EGFR-mutated lung adenocarcinoma, and several studies have shown that image features extracted from ^{18}F-FDG PET are associated with EGFR mutation status [34–36]. In addition, ^{18}F-FDG PET derived radiomic features have been shown to anticipate the treatment response to TKIs in EGFR-mutated lung cancer [37–41]. However, the prognostic value of ^{18}F-FDG PET-based radiomic features for the survival of lung cancer patients treated by EGFR-targeting TKIs has not been well investigated. In this study, we found that the SUV entropy measured from the pretreatment ^{18}F-FDG PET was independently associated with the time-to-progression of EGFR-targeted TKI treatment and the OS in patients with lung adenocarcinoma harboring EGFR mutations. The combination of the ^{18}F-FDG PET radiomic feature and clinical factor allows better survival stratification.

Since tumor heterogeneity results from genomic inhomogeneity and evolution of clones, targetable EGFR mutation may co-exist with non-targetable mutations such as T790M [6, 18, 42–44]. Therefore, the biopsy specimen may be inadequate, and it may be impossible to

Table 2. Univariate and multivariate Cox regression analysis for prognostic factors of survival outcome (n = 51).

Variable	No.	OS				PFS			
		Univariate		Multivariate		Univariate		Multivariate	
		HR (95% CI)	p-value	HR (95% CI)	p-value	HR (95% CI)	p-value	HR (95% CI)	p-value
T4 disease			0.977		NA		0.726		NA
Yes	21	1.0 (0.5–1.9)				1.1 (0.6–2.0)			
No	30	Reference				Reference			
N3 disease			0.959		NA		0.091		NA
Yes	25	1.0 (0.5–1.9)				1.6 (0.9–2.9)			
No	26	Reference				Reference			
M1 disease			0.025		0.166		0.174		NA
Yes	39	2.7 (1.1–6.6)				1.6 (0.8–3.4)			
No	12	Reference				Reference			
Mutation type			0.261		NA		0.467		NA
Deletion 19	23	0.7 (0.4–1.3)				0.8 (0.4–1.4)			
Others	28	Reference				Reference			
Pleural effusion			0.037		< 0.001		0.044		0.003
Presence	20	2.0 (1.1–3.7)		4.0 (1.9–8.5)		1.8 (1.0–3.3)		2.7 (1.4–5.2)	
Absence	31	Reference		Reference		Reference		Reference	
Lung metastasis			0.938		NA		0.742		NA
Presence	19	1.0 (0.5–1.9)				1.1 (0.6–2.0)			
Absence	32	Reference				Reference			
Hepatic metastasis			0.026		0.903		0.234		NA
Presence	6	2.8 (1.1–6.9)				1.7 (0.7–4.2)			
Absence	45	Reference				Reference			
Skeletal metastasis			0.491		NA		0.267		NA
Presence	14	1.3 (0.6–2.6)				1.4 (0.8–2.7)			
Absence	37	Reference				Reference			
Brain metastasis			0.806		NA		0.579		NA
Presence	6	1.1 (0.4–3.2)				1.3 (0.5–3.0)			
Absence	45	Reference				Reference			
SUVmax			0.018		0.166		0.140		NA
> 6.75	13	2.7 (1.2–6.3)				1.7 (0.8–3.2)			
≤ 6.75	38	Reference				Reference			
TLG			0.002		0.739		0.074		NA
> 101	24	3.0 (1.5–5.9)				1.7 (1.0–3.0)			
≤ 101	27	Reference				Reference			
SUV entropy			0.002		<0.001		0.018		0.001
> 5.36	27	2.9 (1.5–5.7)		5.5 (2.5–12.2)		2.0 (1.1–3.6)		2.9 (1.5–5.5)	
≤ 5.36	24	Reference		Reference		Reference		Reference	
Sum entropy			0.001		0.841		0.063		0.586
> 5.8	21	3.5 (1.7–7.2)				1.7 (1.0–3.1)			
≤ 5.8	30	Reference				Reference			
SAE			0.021		0.783		0.195		NA
≤ 0.845	34	2.3 (1.1–4.5)				1.5 (0.8–2.8)			
> 0.845	17	Reference				Reference			

HR: Hazard ratio, CI: Confidence interval, OS: Overall survival, PFS: Progression-free survival, TLG: Total lesion glycolysis, SAE: Small zone emphasis.
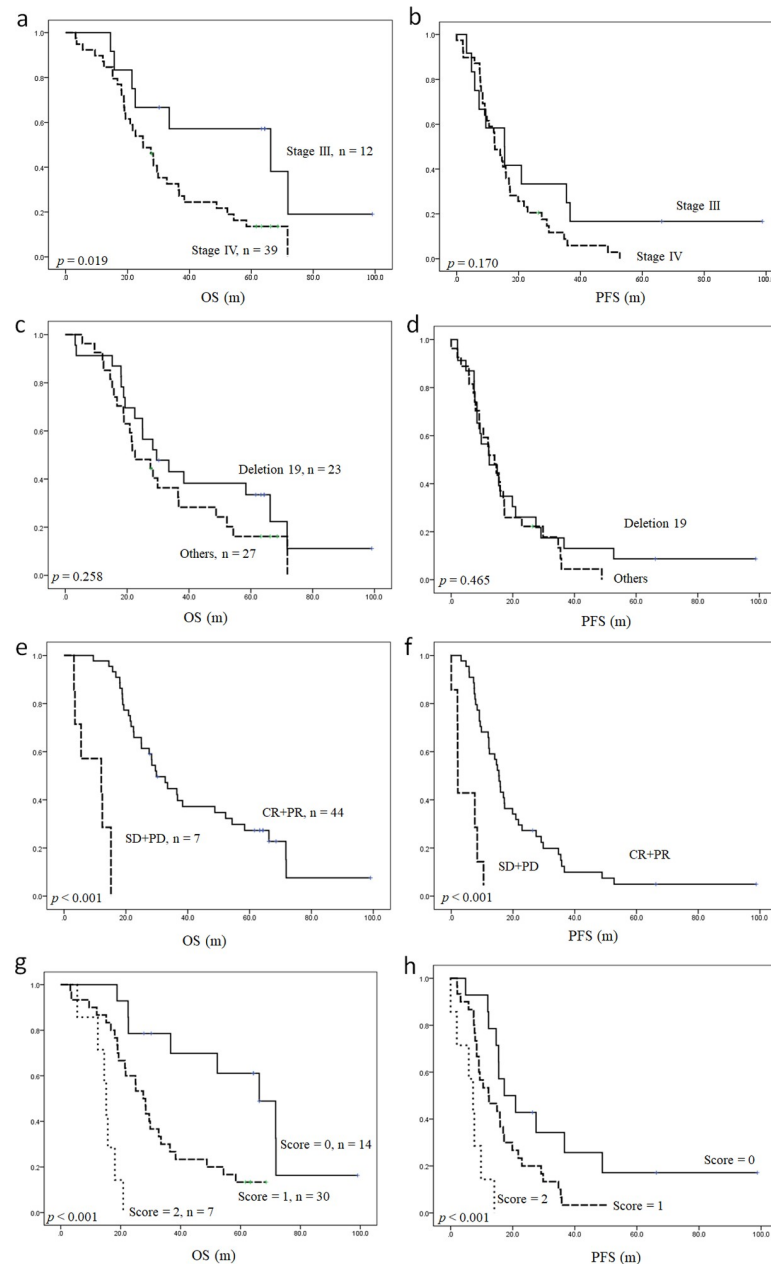
Fig 2. Kaplan-Meier curves presenting OS and PFS in patients with EGFR-mutated lung adenocarcinoma.
Survival stratification according to the traditional TNM staging system (a and b), EGFR mutation status (c and d),
treatment response based on RECIST 1.1 criteria (e and f), and the scoring system developed in the present study (g
and h). OS: Overall survival, PFS: Progression-free survival, EGFR: Epidermal growth factor receptor, CR: Complete
remission, PR: Partial response, SD: Stable disease, PD: Progressive disease.

thoroughly study the EGFR mutation characteristics of the entire tumor. Inadequacy of biopsy
has been demonstrated in the work of Kuiper et al., wherein it was reported that the T790M
status in the re-biopsied lung cancer specimens showed contradictory results in 37% of cases
[45]. In addition, according to the recent molecular-pathological profiling studies for advanced
EGFR mutation-positive non-small cell lung cancer at baseline, the coexisting multiple genetic,
phenotypic, and functional mechanisms may contribute to disease progression and cause
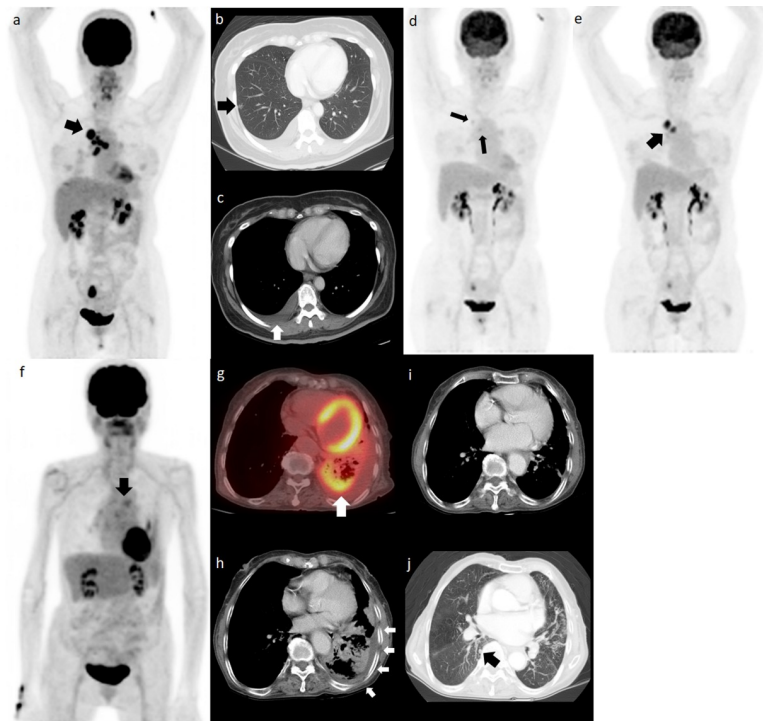
Fig 3. The survival prediction model outperforms the TNM staging system. Pretreatment ^{18}F-FDG PET MIP image (a) for a 58-year-old woman with a primary tumor in the right upper lobe. Because of the presence of tiny nodule in different ipsilateral lobe and malignant pleural effusion (b and c, arrow), the clinical staging was cT4N3M1a. The EGFR mutation was L858R. The SUV entropy of the primary tumor was 5.32 (0.04 lower than the cut-off). A score of 1 was assigned for this patient. After 1 year of erlotinib treatment, the ^{18}F-FDG PET MIP image (d) showed remarkable resolution of the primary tumor and metastatic lymph node ^{18}F-FDG uptake (arrows). The patient experienced disease progression after 29.8 months of first line erlotinib treatment (e, arrow) and the treatment changed to osimertinib thereafter. The patient died of lung cancer with a PFS and OS of 29.8 and 54.3 months, respectively. The pretreatment ^{18}F-FDG PET/CT and MIP images from an 83-year-old woman revealed mediastinal lymph node metastases (f, arrow) and an ^{18}F-FDG avid tumor in the left lower lung (g, arrow). The patient also demonstrated malignant pleural effusion (h, arrows). Her clinical staging was cT3N3M1a and she had a deletion 19 EGFR mutation. The primary tumor SUV entropy was 5.44 (0.08 higher than the cut-off) and a score of 2 was given for this patient. She received erlotinib as a first line therapy. The CT acquired at 6 months after erlotinib treatment (i) showed resolution of the left pleural fluid; however, a new pulmonary nodule developed in the contralateral lung after 9.8 months of erlotinib treatment (j, arrow). The patient died of lung cancer progression with an OS of 18.1 months. MIP: Maximum intensity projection, PET: Positron emission tomography, EGFR: Epidermal growth factor receptor, PFS: Progression-free survival, OS: Overall survival.

https://doi.org/10.1371/journal.pone.0244502.g003

Table 3. Comparison of the c-indices of different survival prediction models (n = 51).

Model	c-index for OS	*p* value[a]	c-index for PFS	*p* value[a]
Our prediction model	0.691	NA	0.649	NA
TNM staging system[b]	0.574	0.013	0.517	0.004
Mutation type of EGFR[c]	0.549	0.003	0.515	0.001
Treatment response[d]	0.625	0.184	0.598	0.210

OS: Overall survival, PFS: Progression-free survival, NA: Not applicable.

[a]Compared to our prediction model.

[b]Staging was based on the 7th American Joint Committee on Cancer system.

[c]Stratified according to the presence or absence of the exon 19 deletion.

[d]Response assessment was based on RECIST 1.1 criteria.

https://doi.org/10.1371/journal.pone.0244502.t003

intrinsic TKI resistance [46]. The advantage of extracting radiomics from ^{18}F-FDG PET is the ability to analyze the entire tumor's heterogeneity, which circumvents the potential prejudice of focal biopsy. The radiomic features of ^{18}F-FDG PET have been shown to correlate with genetic heterogeneity [47] and may serve as a surrogate marker for intratumoral heterogeneity or mutation. Higher heterogeneity may be associated with a higher likelihood of hidden non-targetable EGFR mutations. Therefore, radiomic analysis of ^{18}F-FDG PET may surreptitiously pick out those with hidden non-targetable EGFR mutations and enable the stratification of patients into different risk groups.

Han et al. conducted a systemic review to summarize the prognostic value of radiomics of ^{18}F-FDG PET in lung cancer. In their study, although many radiomics parameters showed prognostic significance, these parameters were not replicated across different studies [17]. Although discrepant results in the studies may be partially attributed to different cancer histology and AJCC staging status, the radiomic feature per se may also contribute to this discrepancy. Since radiomic features of ^{18}F-FDG PET demonstrate diverse repeatability and reliability, selecting features with high reproducibility and high robustness is essential to ensure reliable data output [29, 48, 49]. In our study, the radiomic features selected for analysis have been reported to show high repeatability among different matrices [29]. We found that SUV entropy (a first-order feature) was an independent predictor of survival; this feature has been reported to be repeatable in different image reconstruction methods and resampling methods, and showed good interclass correlation in the test-retest examination [50–52].

The presence of pleural effusion was another independent prognostic factor for OS and PFS in our study. The prognostic value of pleural effusion has been reported in both non-small cell lung cancer and small cell lung cancer [22, 23, 53, 54]. Pleural effusion in patients with lung cancer can directly result from pleural invasion or an indirect consequence of other pathological processes such as mediastinal nodal involvement. Effusion without tumor cell on the pathological exam may also represent an early phase in the development of malignant pleural effusion [23, 53, 55]. In addition, the work by Chen et al.'s showed that the cancer stem cells in lung adenocarcinoma-related pleural effusion were associated with distant metastasis and unfavorable survival. The negative prognostic effect of cancer stem cells might result from the epithelial-mesenchymal transition and adaptation in the cancer microenvironment [56]. Therefore, the presence of pleural effusion may be regarded as a clinical factor of tumor invasion, metastasis, and a more substantial disease burden.

The presence of pleural effusion (clinical factor) and the radiomics derived from the ^{18}F-FDG PET represent distinct biological characteristics of cancer. Pleural effusion reflects tumor invasiveness in the microenvironment, as well as the disease burden [22, 23, 53–56]. In contrast, radiomic feature describes heterogeneity, and is closely related to tumor evolution [18, 19]. Based on these philosophies, the clinical factor and radiomic feature of ^{18}F-FDG PET may be complementary in anticipating the survival prognosis. Therefore, incorporating the two factors may achieve a better survival prediction. However, the prognostic role of combining clinical factor and radiomics of ^{18}F-FDG PET in EGFR-mutated lung cancer has not been thoroughly studied. We found that the combination of pleural effusion and pretreatment primary tumor SUV entropy improved survival stratification. Based on this, we developed a model with a score of 0–2 for predicting OS and PFS according to the number of independent prognosticators present. This survival model showed a significantly higher capability to stratify the survival of patients than the traditional AJCC staging system and the EGFR mutation status. The predictive power of our model was also better than the RECIST system (Table 3), which offers an opportunity to select a risk-directed treatment strategy earlier.

Currently, the time-to-progression of TKI therapy in actionable EGFR mutations is heterogeneous, and there is no reliable model to predict drug resistance or treatment failure

before the start of TKI treatment [6]. New therapeutic strategies have been designed to overcome resistance and improve survival time. For example, initial treatment with the third-generation TKI, osimertinib has gained success in improving survival in EGFR-mutated lung cancer, possibly due to the suppression of tumors harboring hidden T790M mutation [57]. Moreover, the addition of anti-angiogenesis agents to standard TKI also shows PFS benefit [58–60]. In addition, a recent study discovered that the TKI resistance pathway is associated with increased PD-L1 (programmed death-ligand 1) expression [61]. Treatment combination with immune modulation may become another choice [62]. However, in the era of precision medicine, more sophisticated patient stratification is pivotal, and add-on therapy in patients with an excellent response to standard TKI may be obviated. Therefore, our prediction model may be used to stratify patients into different risk groups before the initiation of TKI therapy (Fig 4).

Cook et al. have reported that the interval change of ^{18}F-FDG PET radiomic feature, instead of pretreatment feature, independently predicted the early treatment response to TKI at 12 weeks [41]. Our data are in agreement with these results and showed that pretreatment radiomic features were not significantly associated with the early response (S2 Table). Additional studies with a larger study population are required to investigate whether the combination of pretreatment and interim ^{18}F-FDG PET may further refine the prognostic stratification for both treatment response and survival of lung cancer patients treated with TKIs.

There were several limitations in our study. First, our study cohort was relatively small. Second, this was a retrospective study, and we can not avoid the bias associated with the retrospective review process. Finally, we only performed internal validation for our survival prediction model. The generalizability of our survival prediction model should be prospectively validated using a larger external cohort.

Conclusion

The preliminary data of our study indicate that primary tumor SUV entropy and pleural effusion were early predictive biomarkers of survival in patients with lung adenocarcinoma treated with EGFR-targeted TKIs. The combination of this PET radiomic feature with clinical risk factor yielded a better prognostic stratification model. Our proposed scoring model may enable tailored treatment approaches in patients with EGFR-mutated lung adenocarcinoma treated with standard TKI.
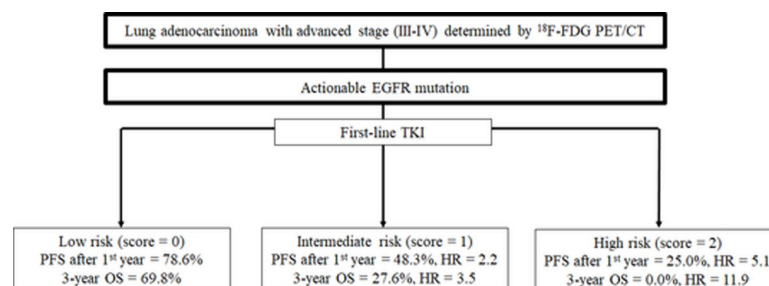
Fig 4. Flow chart illustrating the potential utility of our scoring system in the management of patients with EGFR-mutated lung adenocarcinoma treated with TKI. EGFR: Epidermal growth factor receptor, TKI: Tyrosine kinase inhibitor, PFS: Progression-free survival, OS: Overall survival, HR: Hazard ratio.

https://doi.org/10.1371/journal.pone.0244502.g004

Supporting information

S1 Fig. An example of obtaining the cut-off value from a continuous variable. We tested different cut-off values for the SUV entropy using the log-rank test based on the overall survival rates. Serial chi-square values were obtained, and we choose the cut-off value with the highest chi-square value for further analysis (arrow, SUV entropy cut-off at 5.36 with a chi-square value of 9.82).
(TIF)

S1 Table. Results of the bootstrapping validation of the prediction model. OS: Overall survival, PFS: Progression-free survival, 95% CI: Bias corrected accelerated 95% confidence interval, SE: Standard error.
(DOCX)

S2 Table. Association of clinical and pretreatment imaging variables with the treatment response (n = 51). SD: Stable disease, PD: Progressive disease, OR: Odds ratio, NA: Not applicable. [a]Response assessment was based on RECIST 1.1 criteria. [b]Fisher's exact test.
(DOCX)

Acknowledgments

Author Contributions

Conceptualization: Yu-Hung Chen, Tso-Fu Wang, Kun-Han Lue, Sheng-Chieh Chan.

Data curation: Yu-Hung Chen, Tso-Fu Wang, Sheng-Chieh Chan.

Formal analysis: Yu-Hung Chen, Kun-Han Lue.

Investigation: Yu-Hung Chen, Ling-Yi Wang, Kun-Han Lue, Sheng-Chieh Chan.

Methodology: Yu-Hung Chen, Tso-Fu Wang, Sung-Chao Chu, Ling-Yi Wang, Sheng-Chieh Chan.

Project administration: Yu-Hung Chen.

Software: Yu-Hung Chen, Ling-Yi Wang, Kun-Han Lue.

Supervision: Tso-Fu Wang, Sung-Chao Chu, Ling-Yi Wang, Sheng-Chieh Chan.

Validation: Yu-Hung Chen.

Visualization: Yu-Hung Chen, Sheng-Chieh Chan.

Writing – original draft: Yu-Hung Chen, Sheng-Chieh Chan.

Writing – review & editing: Sung-Chao Chu, Chih-Bin Lin, Shu-Hsin Liu, Sheng-Chieh Chan.

References

1. Torre LA, Bray F, Siegel RL, Ferlay J, Lortet-Tieulent J, Jemal A. Global cancer statistics, 2012. CA Cancer J Clin. 2015; 65(2):87–108. https://doi.org/10.3322/caac.21262 PMID: 25651787

2. Siegel RL, Miller KD, Jemal A. Cancer statistics, 2019. CA Cancer J Clin. 2019; 69(1):7–34. https://doi.org/10.3322/caac.21551 PMID: 30620402

3. Janssen-Heijnen ML, Coebergh JW, Klinkhamer PJ, Schipper RM, Splinter TA, Mooi WJ. Is there a common etiology for the rising incidence of and decreasing survival with adenocarcinoma of the lung? Epidemiology. 2001; 12(2):256–8. https://doi.org/10.1097/00001648-200103000-00020 PMID: 11246589

4. Tsim S, O'Dowd CA, Milroy R, Davidson S. Staging of non-small cell lung cancer (NSCLC): a review. Respir Med. 2010; 104(12):1767–74. https://doi.org/10.1016/j.rmed.2010.08.005 PMID: 20833010

5. Gerber DE, Gandhi L, Costa DB. Management and future directions in non-small cell lung cancer with known activating mutations. Am Soc Clin Oncol Educ Book. 2014:e353–65. https://doi.org/10.14694/EdBook_AM.2014.34.e353 PMID: 24857124

6. Shea M, Costa DB, Rangachari D. Management of advanced non-small cell lung cancers with known mutations or rearrangements: latest evidence and treatment approaches. Ther Adv Respir Dis. 2016; 10(2):113–29. https://doi.org/10.1177/1753465815617871 PMID: 26620497

7. Gridelli C, De Marinis F, Di Maio M, Cortinovis D, Cappuzzo F, Mok T. Gefitinib as first-line treatment for patients with advanced non-small-cell lung cancer with activating epidermal growth factor receptor mutation: Review of the evidence. Lung Cancer. 2011; 71(3):249–57. https://doi.org/10.1016/j.lungcan.2010.12.008 PMID: 21216486

8. Lynch TJ, Bell DW, Sordella R, Gurubhagavatula S, Okimoto RA, Brannigan BW, et al. Activating mutations in the epidermal growth factor receptor underlying responsiveness of non-small-cell lung cancer to gefitinib. N Engl J Med. 2004; 350(21):2129–39. https://doi.org/10.1056/NEJMoa040938 PMID: 15118073

9. Lindeman NI, Cagle PT, Beasley MB, Chitale DA, Dacic S, Giaccone G, et al. Molecular testing guideline for selection of lung cancer patients for EGFR and ALK tyrosine kinase inhibitors: guideline from the College of American Pathologists, International Association for the Study of Lung Cancer, and Association for Molecular Pathology. Arch Pathol Lab Med. 2013; 137(6):828–60. https://doi.org/10.5858/arpa.2012-0720-OA PMID: 23551194

10. Cuaron J, Dunphy M, Rimner A. Role of FDG-PET scans in staging, response assessment, and follow-up care for non-small cell lung cancer. Front Oncol. 2012; 2:208. https://doi.org/10.3389/fonc.2012.00208 PMID: 23316478

11. Steinert HC. PET in lung cancer. Chang Gung Med J. 2005; 28(5):296–305. PMID: 16086544

12. Yoo Ie R, Chung SK, Park HL, Choi WH, Kim YK, Lee KY, et al. Prognostic value of SUVmax and metabolic tumor volume on 18F-FDG PET/CT in early stage non-small cell lung cancer patients without LN metastasis. Biomed Mater Eng. 2014; 24(6):3091–103. https://doi.org/10.3233/BME-141131 PMID: 25227018

13. Takeda A, Yokosuka N, Ohashi T, Kunieda E, Fujii H, Aoki Y, et al. The maximum standardized uptake value (SUVmax) on FDG-PET is a strong predictor of local recurrence for localized non-small-cell lung cancer after stereotactic body radiotherapy (SBRT). Radiother Oncol. 2011; 101(2):291–7. https://doi.org/10.1016/j.radonc.2011.08.008 PMID: 21889224

14. Park SY, Cho A, Yu WS, Lee CY, Lee JG, Kim DJ, et al. Prognostic value of total lesion glycolysis by 18F-FDG PET/CT in surgically resected stage IA non-small cell lung cancer. J Nucl Med. 2015; 56 (1):45–9. https://doi.org/10.2967/jnumed.114.147561 PMID: 25525185

15. Takeda K, Takanami K, Shirata Y, Yamamoto T, Takahashi N, Ito K, et al. Clinical utility of texture analysis of 18F-FDG PET/CT in patients with Stage I lung cancer treated with stereotactic body radiotherapy. J Radiat Res. 2017; 58(6):862–9. https://doi.org/10.1093/jrr/rrx050 PMID: 29036692

16. Pyka T, Bundschuh RA, Andratschke N, Mayer B, Specht HM, Papp L, et al. Textural features in pre-treatment [F18]-FDG-PET/CT are correlated with risk of local recurrence and disease-specific survival in early stage NSCLC patients receiving primary stereotactic radiation therapy. Radiat Oncol. 2015; 10:100. https://doi.org/10.1186/s13014-015-0407-7 PMID: 25900186

17. Han S, Woo S, Suh CH, Kim YJ, Oh JS, Lee JJ. A systematic review of the prognostic value of texture analysis in (18)F-FDG PET in lung cancer. Ann Nucl Med. 2018; 32(9):602–10. https://doi.org/10.1007/s12149-018-1281-9 PMID: 30014440

18. Caswell DR, Swanton C. The role of tumour heterogeneity and clonal cooperativity in metastasis, immune evasion and clinical outcome. BMC Med. 2017; 15(1):133. https://doi.org/10.1186/s12916-017-0900-y PMID: 28716075

19. McGranahan N, Swanton C. Clonal Heterogeneity and Tumor Evolution: Past, Present, and the Future. Cell. 2017; 168(4):613–28. https://doi.org/10.1016/j.cell.2017.01.018 PMID: 28187284

20. Yip C, Landau D, Kozarski R, Ganeshan B, Thomas R, Michaelidou A, et al. Primary esophageal cancer: heterogeneity as potential prognostic biomarker in patients treated with definitive chemotherapy and radiation therapy. Radiology. 2014; 270(1):141–8. https://doi.org/10.1148/radiol.13122869 PMID: 23985274

21. Jiangdian S, Di D, Yanqi H, Yali Z, Zaiyi L, Jie T. Association between tumor heterogeneity and progression-free survival in non-small cell lung cancer patients with EGFR mutations undergoing tyrosine kinase inhibitors therapy. Conf Proc IEEE Eng Med Biol Soc. 2016; 2016:1268–71.

22. Lim E, Clough R, Goldstraw P, Edmonds L, Aokage K, Yoshida J, et al. Impact of positive pleural lavage cytology on survival in patients having lung resection for non-small-cell lung cancer: An international individual patient data meta-analysis. J Thorac Cardiovasc Surg. 2010; 139(6):1441–6. https://doi.org/10.1016/j.jtcvs.2009.05.048 PMID: 19939412

23. Ryu JS, Lim JH, Lee JM, Kim WC, Lee KH, Memon A, et al. Minimal Pleural Effusion in Small Cell Lung Cancer: Proportion, Mechanisms, and Prognostic Effect. Radiology. 2016; 278(2):593–600. https://doi.org/10.1148/radiol.2015142388 PMID: 26323029

24. Lapa P, Marques M, Isidoro J, Barata F, Costa G, de Lima JP. (18)F-FDG PET/CT in lung cancer. The added value of quantification. Rev Esp Med Nucl Imagen Mol. 2017; 36(6):342–9. https://doi.org/10.1016/j.remn.2017.04.001 PMID: 28566260

25. Cheng NM, Fang YH, Lee LY, Chang JT, Tsan DL, Ng SH, et al. Zone-size nonuniformity of 18F-FDG PET regional textural features predicts survival in patients with oropharyngeal cancer. Eur J Nucl Med Mol Imaging. 2015; 42(3):419–28. https://doi.org/10.1007/s00259-014-2933-1 PMID: 25339524

26. Chen YH, Lue KH, Chu SC, Chang BS, Wang LY, Liu DW, et al. Combining the radiomic features and traditional parameters of (18)F-FDG PET with clinical profiles to improve prognostic stratification in patients with esophageal squamous cell carcinoma treated with neoadjuvant chemoradiotherapy and surgery. Ann Nucl Med. 2019; 33(9):657–70. https://doi.org/10.1007/s12149-019-01380-7 PMID: 31218571

27. Cheng NM, Fang YH, Chang JT, Huang CG, Tsan DL, Ng SH, et al. Textural features of pretreatment 18F-FDG PET/CT images: prognostic significance in patients with advanced T-stage oropharyngeal squamous cell carcinoma. J Nucl Med. 2013; 54(10):1703–9. https://doi.org/10.2967/jnumed.112.119289 PMID: 24042030

28. Orlhac F, Soussan M, Maisonobe JA, Garcia CA, Vanderlinden B, Buvat I. Tumor texture analysis in 18F-FDG PET: relationships between texture parameters, histogram indices, standardized uptake values, metabolic volumes, and total lesion glycolysis. J Nucl Med. 2014; 55(3):414–22. https://doi.org/10.2967/jnumed.113.129858 PMID: 24549286

29. Desseroit MC, Tixier F, Weber WA, Siegel BA, Cheze Le Rest C, Visvikis D, et al. Reliability of PET/CT Shape and Heterogeneity Features in Functional and Morphologic Components of Non-Small Cell Lung Cancer Tumors: A Repeatability Analysis in a Prospective Multicenter Cohort. J Nucl Med. 2017; 58(3):406–11. https://doi.org/10.2967/jnumed.116.180919 PMID: 27765856

30. van Griethuysen JJM, Fedorov A, Parmar C, Hosny A, Aucoin N, Narayan V, et al. Computational Radiomics System to Decode the Radiographic Phenotype. Cancer Res. 2017; 77(21):e104–e7. https://doi.org/10.1158/0008-5472.CAN-17-0339 PMID: 29092951

31. Schwartz LH, Litiere S, de Vries E, Ford R, Gwyther S, Mandrekar S, et al. RECIST 1.1-Update and clarification: From the RECIST committee. Eur J Cancer. 2016; 62:132–7. https://doi.org/10.1016/j.ejca.2016.03.081 PMID: 27189322

32. Camp RL, Dolled-Filhart M, Rimm DL. X-tile: a new bio-informatics tool for biomarker assessment and outcome-based cut-point optimization. Clin Cancer Res. 2004; 10(21):7252–9. https://doi.org/10.1158/1078-0432.CCR-04-0713 PMID: 15534099

33. Kang L, Chen W, Petrick NA, Gallas BD. Comparing two correlated C indices with right-censored survival outcome: a one-shot nonparametric approach. Stat Med. 2015; 34(4):685–703. https://doi.org/10.1002/sim.6370 PMID: 25399736

34. Koyasu S, Nishio M, Isoda H, Nakamoto Y, Togashi K. Usefulness of gradient tree boosting for predicting histological subtype and EGFR mutation status of non-small cell lung cancer on (18)F FDG-PET/CT. Ann Nucl Med. 2020; 34(1):49–57. https://doi.org/10.1007/s12149-019-01414-0 PMID: 31659591

35. Zhang J, Zhao X, Zhao Y, Zhang J, Zhang Z, Wang J, et al. Value of pre-therapy (18)F-FDG PET/CT radiomics in predicting EGFR mutation status in patients with non-small cell lung cancer. Eur J Nucl Med Mol Imaging. 2019. https://doi.org/10.1007/s00259-019-04592-1 PMID: 31728587

36. Li X, Yin G, Zhang Y, Dai D, Liu J, Chen P, et al. Predictive Power of a Radiomic Signature Based on (18)F-FDG PET/CT Images for EGFR Mutational Status in NSCLC. Front Oncol. 2019; 9:1062. https://doi.org/10.3389/fonc.2019.01062 PMID: 31681597

37. van Gool MH, Aukema TS, Hartemink KJ, Valdes Olmos RA, van Tinteren H, Klomp HM. FDG-PET/CT response evaluation during EGFR-TKI treatment in patients with NSCLC. World J Radiol. 2014; 6(7):392–8. https://doi.org/10.4329/wjr.v6.i7.392 PMID: 25071879

38. Koizumi T, Fukushima T, Gomi D, Kobayashi T, Sekiguchi N, Mamiya K, et al. Correlation of early PET findings with tumor response to molecular targeted agents in patients with advanced driver-mutated non-small cell lung cancer. Med Oncol. 2017; 34(10):169. https://doi.org/10.1007/s12032-017-1032-0 PMID: 28864950

39. Kus T, Aktas G, Sevinc A, Kalender ME, Yilmaz M, Kul S, et al. Prognostic impact of initial maximum standardized uptake value of (18)F-FDG PET/CT on treatment response in patients with metastatic

lung adenocarcinoma treated with erlotinib. Onco Targets Ther. 2015; 8:3749–56. https://doi.org/10.2147/OTT.S94945 PMID: 26719702

40. van Gool MH, Aukema TS, Sinaasappel M, Valdes Olmos RA, Klomp HM. Tumor heterogeneity on (18) F-FDG-PET/CT for response monitoring in non-small cell lung cancer treated with erlotinib. J Thorac Dis. 2016; 8(3):E200–3. https://doi.org/10.21037/jtd.2016.02.10 PMID: 27076970

41. Cook GJ, O'Brien ME, Siddique M, Chicklore S, Loi HY, Sharma B, et al. Non-Small Cell Lung Cancer Treated with Erlotinib: Heterogeneity of (18)F-FDG Uptake at PET-Association with Treatment Response and Prognosis. Radiology. 2015; 276(3):883–93. https://doi.org/10.1148/radiol.2015141309 PMID: 25897473

42. Su KY, Chen HY, Li KC, Kuo ML, Yang JC, Chan WK, et al. Pretreatment epidermal growth factor receptor (EGFR) T790M mutation predicts shorter EGFR tyrosine kinase inhibitor response duration in patients with non-small-cell lung cancer. J Clin Oncol. 2012; 30(4):433–40. https://doi.org/10.1200/JCO.2011.38.3224 PMID: 22215752

43. Yap TA, Gerlinger M, Futreal PA, Pusztai L, Swanton C. Intratumor heterogeneity: seeing the wood for the trees. Sci Transl Med. 2012; 4(127):127ps10. https://doi.org/10.1126/scitranslmed.3003854 PMID: 22461637

44. Yu JY, Yu SF, Wang SH, Bai H, Zhao J, An TT, et al. Clinical outcomes of EGFR-TKI treatment and genetic heterogeneity in lung adenocarcinoma patients with EGFR mutations on exons 19 and 21. Chin J Cancer. 2016; 35:30. https://doi.org/10.1186/s40880-016-0086-2 PMID: 27001083

45. Kuiper JL, Heideman DA, Thunnissen E, Paul MA, van Wijk AW, Postmus PE, et al. Incidence of T790M mutation in (sequential) rebiopsies in EGFR-mutated NSCLC-patients. Lung Cancer. 2014; 85 (1):19–24. https://doi.org/10.1016/j.lungcan.2014.03.016 PMID: 24768581

46. Santoni-Rugiu E, Melchior LC, Urbanska EM, Jakobsen JN, Stricker K, Grauslund M, et al. Intrinsic resistance to EGFR-Tyrosine Kinase Inhibitors in EGFR-Mutant Non-Small Cell Lung Cancer: Differences and Similarities with Acquired Resistance. Cancers (Basel). 2019; 11(7). https://doi.org/10.3390/cancers11070923 PMID: 31266248

47. Moon SH, Kim J, Joung JG, Cha H, Park WY, Ahn JS, et al. Correlations between metabolic texture features, genetic heterogeneity, and mutation burden in patients with lung cancer. Eur J Nucl Med Mol Imaging. 2019; 46(2):446–54. https://doi.org/10.1007/s00259-018-4138-5 PMID: 30145701

48. Zwanenburg A. Radiomics in nuclear medicine: robustness, reproducibility, standardization, and how to avoid data analysis traps and replication crisis. Eur J Nucl Med Mol Imaging. 2019; 46(13):2638–55. https://doi.org/10.1007/s00259-019-04391-8 PMID: 31240330

49. Zhuang M, Garcia DV, Kramer GM, Frings V, Smit EF, Dierckx R, et al. Variability and Repeatability of Quantitative Uptake Metrics in (18)F-FDG PET/CT of Non-Small Cell Lung Cancer: Impact of Segmentation Method, Uptake Interval, and Reconstruction Protocol. J Nucl Med. 2019; 60(5):600–7. https://doi.org/10.2967/jnumed.118.216028 PMID: 30389824

50. Leijenaar RT, Carvalho S, Velazquez ER, van Elmpt WJ, Parmar C, Hoekstra OS, et al. Stability of FDG-PET Radiomics features: an integrated analysis of test-retest and inter-observer variability. Acta Oncol. 2013; 52(7):1391–7. https://doi.org/10.3109/0284186X.2013.812798 PMID: 24047337

51. van Velden FH, Kramer GM, Frings V, Nissen IA, Mulder ER, de Langen AJ, et al. Repeatability of Radiomic Features in Non-Small-Cell Lung Cancer [(18)F]FDG-PET/CT Studies: Impact of Reconstruction and Delineation. Mol Imaging Biol. 2016; 18(5):788–95. https://doi.org/10.1007/s11307-016-0940-2 PMID: 26920355

52. Konert T, Everitt S, La Fontaine MD, van de Kamer JB, MacManus MP, Vogel WV, et al. Robust, independent and relevant prognostic 18F-fluorodeoxyglucose positron emission tomography radiomics features in non-small cell lung cancer: Are there any? PLoS One. 2020; 15(2):e0228793. https://doi.org/10.1371/journal.pone.0228793 PMID: 32097418

53. Ryu JS, Ryu HJ, Lee SN, Memon A, Lee SK, Nam HS, et al. Prognostic impact of minimal pleural effusion in non-small-cell lung cancer. J Clin Oncol. 2014; 32(9):960–7. https://doi.org/10.1200/JCO.2013.50.5453 PMID: 24550423

54. Wang TF, Chu SC, Lee JJ, Yang GG, Huang WH, Chang ET, et al. Presence of pleural effusion is associated with a poor prognosis in patients with epidermal growth factor receptor-mutated lung cancer receiving tyrosine kinase inhibitors as first-line treatment. Asia Pac J Clin Oncol. 2017; 13(4):304–13. https://doi.org/10.1111/ajco.12658 PMID: 28124437

55. Light RW, Hamm H. Malignant pleural effusion: would the real cause please stand up? Eur Respir J. 1997; 10(8):1701–2. https://doi.org/10.1183/09031936.97.10081701 PMID: 9272907

56. Chen SF, Lin YS, Jao SW, Chang YC, Liu CL, Lin YJ, et al. Pulmonary Adenocarcinoma in Malignant Pleural Effusion Enriches Cancer Stem Cell Properties during Metastatic Cascade. PLoS One. 2013; 8 (5):e54659. https://doi.org/10.1371/journal.pone.0054659 PMID: 23658677

57. Soria JC, Ohe Y, Vansteenkiste J, Reungwetwattana T, Chewaskulyong B, Lee KH, et al. Osimertinib in Untreated EGFR-Mutated Advanced Non-Small-Cell Lung Cancer. N Engl J Med. 2018; 378(2):113–25. https://doi.org/10.1056/NEJMoa1713137 PMID: 29151359

58. Hata A, Katakami N, Kaji R, Yokoyama T, Kaneda T, Tamiya M, et al. Afatinib plus bevacizumab combination after acquired resistance to EGFR tyrosine kinase inhibitors in EGFR-mutant non-small cell lung cancer: Multicenter, single-arm, phase 2 trial (ABC Study). Cancer. 2018; 124(19):3830–8. https://doi.org/10.1002/cncr.31678 PMID: 30192383

59. Jiang T, Zhang Y, Li X, Zhao C, Chen X, Su C, et al. EGFR-TKIs plus bevacizumab demonstrated survival benefit than EGFR-TKIs alone in patients with EGFR-mutant NSCLC and multiple brain metastases. Eur J Cancer. 2019; 121:98–108. https://doi.org/10.1016/j.ejca.2019.08.021 PMID: 31569068

60. Saito H, Fukuhara T, Furuya N, Watanabe K, Sugawara S, Iwasawa S, et al. Erlotinib plus bevacizumab versus erlotinib alone in patients with EGFR-positive advanced non-squamous non-small-cell lung cancer (NEJ026): interim analysis of an open-label, randomised, multicentre, phase 3 trial. The Lancet Oncology. 2019; 20(5):625–35. https://doi.org/10.1016/S1470-2045(19)30035-X PMID: 30975627

61. Peng S, Wang R, Zhang X, Ma Y, Zhong L, Li K, et al. EGFR-TKI resistance promotes immune escape in lung cancer via increased PD-L1 expression. Mol Cancer. 2019; 18(1):165. https://doi.org/10.1186/s12943-019-1073-4 PMID: 31747941

62. Gettinger S, Hellmann MD, Chow LQM, Borghaei H, Antonia S, Brahmer JR, et al. Nivolumab Plus Erlotinib in Patients With EGFR-Mutant Advanced NSCLC. J Thorac Oncol. 2018; 13(9):1363–72. https://doi.org/10.1016/j.jtho.2018.05.015 PMID: 29802888